INVESTIGATING THE RELATIONSHIP BETWEEN ICE PARTICLES IN CLOUDS AND PRECIPITATION PARTICLES DURING SNOWFALL EVENTS: A CASE STUDY AT SONNBLICK OBSERVATORY, AUSTRIA

Veronika Krieger[1]*, Julia Burkart[2], Christian Maier[2], Thomas Bachleitner[2], Gerhard Schauer[2]

1 GeoSphere Austria – Avalanche Warning Service Salzburg, Salzburg, Austria
2 GeoSphere Austria – Sonnblick Observatory, Salzburg, Austria

ABSTRACT: The Sonnblick Observatory - located at 3,106 m above sea level in the Austrian Alps - provides a unique environment for studying cloud microphysics under in-situ conditions. Operated by the national meteorological service GeoSphere Austria, the observatory is equipped with a wide range of instruments, related to the atmosphere, biosphere and cryosphere. The site combines continuous environmental measurements with year-round human observations of snowfall and snowpack properties. This combination gives us the opportunity to analyze the transformation of ice crystals from their formation through to snowfall.

Snow crystals exhibit a wide range of morphologies depending on temperature and supersaturation. Based on these parameters, the Nakaya diagram offers a long-established classification system of crystal shapes. However, as snow and ice are sensitive to changes in temperature, humidity, evaporation and wind, the structure of the precipitation particles is expected to evolve within the cloud, during their descent through the atmosphere, and after deposition on the snow surface. Because of this complexity, the relationship between ice crystals forming within clouds and snowflakes reaching the surface remains insufficiently understood.

At Sonnblick Observatory small ice crystals (0.5-200µm) within clouds are documented using a measurement device that takes holographic images (SwisensPoleno Jupiter). Meteorological conditions at the observatory are constantly monitored by standardized instruments (WMO Standard). In addition, the shape of the fallen snowflakes is determined and classified through human observation using a snow grid card.

As part of this study, an automatic image classification system was implemented and tested on the holographic images. This made it possible to analyze data across various meteorological conditions and to investigate both how these conditions influence snow crystal shape and how crystals evolve between their formation in clouds and their deposition as snow flake to the surface. Improved understanding of snow crystal evolution can further help us to better comprehend the effects on snowpack formation and its subsequent transformation.

KEYWORDS: ice crystal formation, crystal growth, holographic imaging, Nakaya diagram, in-cloud particles

1. INTRODUCTION

Crystal growth is a fascinating and intricate phenomenon that researchers have investigated extensively, both through laboratory and field experiments (Furukawa, 2015; Libbrecht, 2005; Nakaya, 1954) and through computational modeling approaches (Barrett et al., 2012; Demange et al., 2017; Gravner and Griffeath, 2009; Reiter, 2005) This research has led to a detailed understanding of how and under what conditions certain crystal forms are formed. It is now well established that crystal growth begins with the emergence of hexagonal prisms. These structures act as the basic building blocks from which a wide range of crystal morphologies subsequently emerge (Libbrecht, 2001). Based on these elementary hexagonal prisms the crystals develop into more elaborate, branching dendritic forms. In the atmosphere, this shift tends to happen as the crystals grow larger. In particular, crystals tend to stay in a hexagonal-prism form up to roughly 100 µm in size (Libbrecht, 2005) before they develop into more complex shapes.

* *Corresponding author address:*
Veronika Krieger, GeoSphere Austria, Salzburg, Austria; email: veronika.krieger@geosphere.at

https://doi.org/10.15788/1790099355

The eventual shapes snow crystals take can be systematically sorted into categories based on their form, following the classification scheme laid out by Magono and Lee (1966). Categories such as plates, columns, and needles, among others, arise from the particular environmental conditions under which the crystals formed. A well-known tool for capturing this relationship is the Nakaya morphology diagram, originally proposed by Nakaya (1954) and later extended by Kobayashi (1961), which maps out in detail how atmospheric factors, particularly temperature and supersaturation, shape which snow crystal form develops.

Several case studies confirm the relationship between meteorological environmental conditions and different ice crystal shapes (Bailey and Hallett, 2009; Pasquier et al., 2023). Under laboratory conditions, the correlation is evident; in real-world studies, however, individual ice crystals are subjected to changing environmental conditions. The study by Krieger et al. (2024), which analyzes data from a holographic measurement device (SwisensPoleno Jupiter), shows good agreement between the captured crystals and the Nakaya diagram. However, the study also mentions some differences between the ice particles floating in the cloud and the snowflakes that fall as snow.

By introducing an automatic classification of the holographic images this study aims to expand the meteorological regimes under investigation. This method makes it possible to identify discrepancies between observations and theory by analyzing a wide range of data.

2. MEASURING SITE AND METHOD

The Sonnblick Observatory (SBO) is a leading climate and environmental research station, run by GeoSphere Austria and situated atop Mt. Hoher Sonnblick at an elevation of 3,106 meters above sea level. It hosts the ACTRIS European Center for Cloud Ambient Intercomparison (ECCINT), which establishes it as a key site for cutting-edge atmospheric research. SBO carries out continuous monitoring across the atmosphere, cryosphere, and biosphere around the clock. This capability, paired with ECCINT, opens up new analytical possibilities for studying precipitation and deposition processes tied to snow and avalanche conditions. Owing to its elevation, the observatory sits inside clouds much of the time. This gives researchers a rare and valuable window into the fine-scale processes of ice particle formation and growth within clouds, along with the precipitation that follows.

Central to this study is the SwisensPoleno Jupiter (Sauvageat et al., 2020) a state-of-the-art instrument typically used for pollen monitoring. The SwisensPoleno Jupiter is housed in a weatherproof enclosure and mounted outdoors on the Sonnblick measuring platform. It uses holographic imaging to generate detailed images of individual particles that are drawn into its measurement chamber. Air is sampled at a rate of 40 l/min through a Sigma-2 inlet; the instrument is able to detect particles ranging from 0.5 to 200 µm allowing it to capture the smallest ice particles still in the midst of the growth process within a cloud. Each particle is captured holographically from two perpendicular angles, yielding a pair of images. To manage the large volume of data, the images were classified using an automatic classification algorithm.

To determine the environmental conditions under which ice crystals form, meteorological data from automatic weather stations were analyzed. A ceilometer was used to ensure that the SwisensPoleno Jupiter took its measurements inside the cloud. Given the small size of the ice crystals analyzed by the instrument, it is likely that the crystals had remained in the cloud for only a short time (Bailey and Hallett, 2004; Fuchs et al., 2025). Therefore, the station's meteorological data are considered representative of the crystal formation regime.

In our case study, we aimed to analyze crystals at various states of growth. To that end, we compared the holographic images of cloud crystals to visual observations of precipitating snow crystals at the Sonnblick Observatory. To verify image classifications and visual observations, we also conducted a comparison with the Nakaya diagram. The data collection spanned 7 days (Feb 20 to 24 and Mar 22 to 23), with observations divided into 14 distinct periods.

2.1 Automatic Image Classification

Before image classification, fine water droplets as well as low intensity images were filtered out. Water droplets are expected for mixed-phase clouds typically occurring at Mt. Hoher Sonnblick outside of summer. Droplets are typically round and smaller than 20 µm in diameter. In the remaining images noise was reduced and contrast was enhanced using various filters from Python's OpenCV library.

The following analysis of the holographic images was performed with Python using the YOLOv8 embedding model from the Ultralytics library in combination with the machine learning classification model

XGBClassifier from the XGBoost library. To ensure quality, several checks were implemented for both the embedding model and the classifier. For the embedding model, two different versions of the YOLO embedding model were checked. Compared to the newer YOLO26, YOLOv8 demonstrated greater robustness against variations that occurred between measurement periods and was therefore used for further classification. Then, near-duplicate checks were conducted to verify that the algorithm could differentiate between the individual images, ensuring they produced distinct embeddings. Finally, a sanity check verified that similar embeddings were assigned to the same class. The embedding model extracted features from each image, including the manually classified data, and encoded them into an output tensor. For the classification process, 450 of the holographic images were classified manually into 11 classes. Images of four different days were classified to cover as many meteorological conditions as possible. In the images, which show the ice crystals from various angles, the crystals look like plates, dendritic plates, plates in a side-view perspective, H-shapes, diamond forms, rectangles, lines, thick lines, double lines, points or rime (see Figure 1). The manually classified set was split by time slot into training (80%) and validation (20%) data, and the corresponding embeddings were divided accordingly for training and evaluating the classification model. The classification algorithm returns a “best guess” including a confidence score. A threshold was chosen to achieve a classification precision of 0.8. This threshold minimizes incorrect classifications, but it also contributes to some crystals not being classified. Finally, the accuracy of the classification was checked using a confusion matrix, which yielded a value of 0.63. After the classification process, the classes of the two corresponding images for each crystal were combined to determine the actual crystal class according to the main classes (plates, columns, needles, columns with plates or rime) in the classification system proposed by Magono and Lee (1966).

3. RESULTS

Various weather conditions were recorded during the 7 days of observation. Snowfall was analyzed both during the passage of weather fronts and during brief periods of deteriorating weather conditions. Figure 2 shows the changes in temperature, humidity and snow depth throughout the days and highlights the periods analyzed (shaded yellow areas).

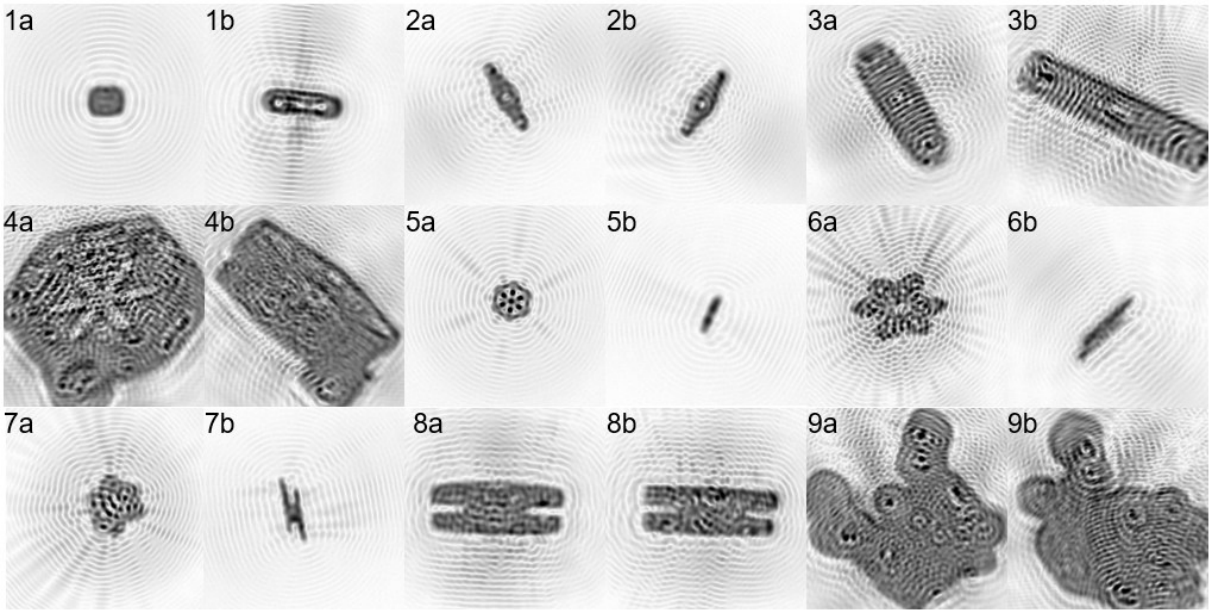


Figure 1: Exemplary holographic images of ice crystals taken by SwisensPoleno Jupiter, the side length of an image is about 200µm; Each pair 1a-1b, 2a-2b, etc., depicts the same ice crystal from different perspectives; 1a: rectangle, 1b: thick line; 2a: diamond shape, 2b: diamond shape; 3a: rectangle, 3b: rectangle; 4a: plate, 4b: plate in a side-view perspective; 5a: plate, 5b: line; 6a: dendritic plate, 6b: double line; 7a: dendritic plate, 7b: H-form; 8a: H-form, 8b: H-form; 9a: rime, 9b: rime.

Over the course of 14 time slots, SwisensPoleno Jupiter recorded a total of 133,784 events, each consisting of a pair of images. Although ice crystals always begin their formation as hexagonal plates and the size of the observed crystals was usually less than 200µm, the images already show different shapes that can be clearly distinguished from one another (see Figure 1 for examples). Nevertheless, many of the photos are unclear; they show water droplets, mixed forms, and sleet.

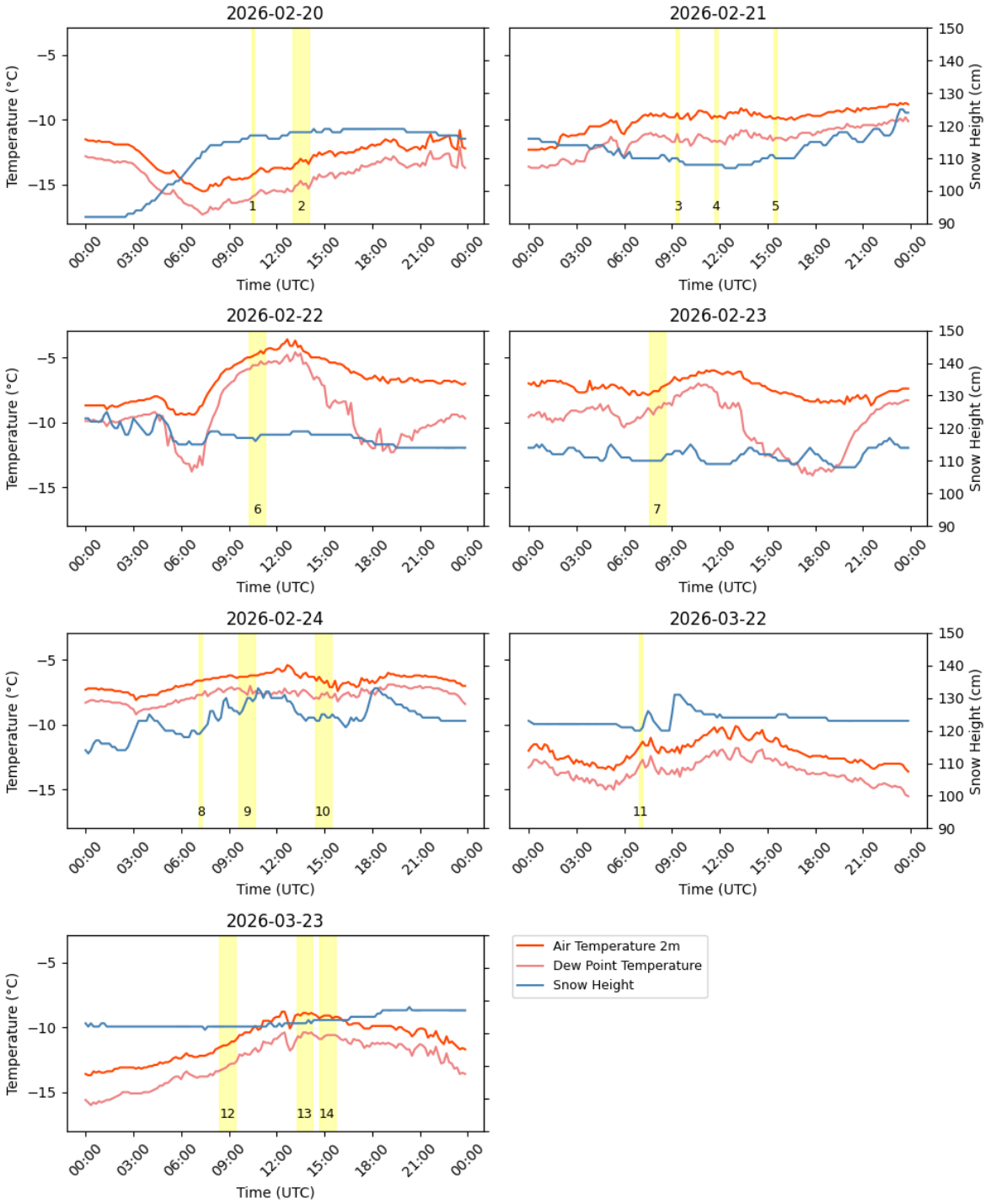


Figure 2: Measurements from automatic weather station at the Sonnblick Observatory in 10-minute intervals. SwisensPoleno Jupiter observation time slots are highlighted in yellow.

Originally, the time period for each time slot was set to 1h around the observation of the falling snow crystals, and the distribution of events over the period was analyzed. However, since some observation periods still had significantly more events to analyze than others after filtering, the time period for these intervals was limited to 10 minutes (see Table 1). To unambiguously classify an ice crystal, the images in each corresponding pair must be assigned to a single class respectively. The combination of these classes then determines the classification as a plate (P), column (C), needle (N), column with plates (CP) or rime (R) according to Magono and Lee (1966); for example, an image pair consisting of two rectangles was classified as column, a pair consisting of two diamonds as needle, and a dendrite combined with a line as plate. It is important to note that, according to Magono and Lee's classification, dendrites are also considered plates; the Nakaya diagram also classifies them under the plate category.

In contrast, needles are listed as a separate form in Magono and Lee's classification, whereas in the Nakaya diagram they are a subtype of columns (Nakaya, 1954).

After filtering the images by particle size and intensity, a total of 35,292 individual images remained for classification. A crystal shape was detected in 12,214 of these images, which ultimately resulted in 2,375 classified crystals. Table 1 shows the filtering and classification statistics for each time slot. There are several reasons why some time slots contain relatively more classifications than others. The SwisensPoleno Jupiter is gently heated, which means it can alter crystals at different rates depending on their size and shape. In addition, certain crystal shapes are simply easier to classify than others. The proportion of classified crystals is consistent with Krieger et al. (2024), in which the entire dataset was classified manually. Figure 3 shows the distribution of the individual crystal forms by time slot. It is evident that the distributions change, with plates, columns, and rime sometimes being the predominant crystal form.

Table 1: Statistics of the filtering and classification process; Events refers to a pair of images.

No.	*Time slot [UTC]*	*Total events*	*Events after automatic filtering*	*Classification single images*	*Classification crystals*	*Percentage of crystal classifications (after filtering)*
1	2026-02-20 10:25-11:35	3925	1336	962	174	13,0
2	2026-02-20 13:00-14:00	19120	404	383	87	21,5
3	2026-02-21 9:15-9:25	2736	681	576	118	17,3
4	2026-02-21 11:40-11:50	3286	1874	1570	313	16,7
5	2026-02-21 15:25-15:35	2000	919	652	109	11,9
6	2026-02-22 10:15-11:15	17174	603	547	78	12,9
7	2026-02-23 7:35-8:35	8571	2359	2306	567	24,0
8	2026-02-24 7:08-7:18	3866	706	635	125	17,7
9	2026-02-24 9:38-10:38	18838	3370	335	68	2,0
10	2026-02-24 14:25-15:25	17851	947	943	183	19,3
11	2026-03-22 6:57-7:07	2483	836	624	124	14,8
12	2026-03-23 8:25-9:25	11947	2518	1568	210	8,3
13	2026-03-23 13:15-14:15	9723	639	602	107	16,7
14	2026-03-23 14:41-15:41	12264	454	511	112	24,7

Comparing the three data sources (visual ground observations, the SwisensPoleno Jupiter classification, and the theoretical predictions from the Nakaya diagram) plates stand out as the case of clearest agreement, while other crystal types show greater discrepancies (see Table 2). For the first two time slots, ground observations, the classification, and the Nakaya diagram all consistently point to plates. However, the Nakaya diagram also suggests plates for time slot 11 and 12 whereas the visual observations show dendrites for both and the classification confirms plates in time slot 11 but suggests columns in time slot 12. Nevertheless, the fact that time windows 1 and 2 coincide across all three independent methods suggests that plates are the most reliably identified crystal type in this dataset. Analysis of Figure 3 and Figure 4 reveals that the correlation is highest the higher the relative humidity over ice is. Some level of agreement is also found for rimed particles. On February 24 (time slot 8 to 10), observations showed rimed particles, sometimes in such large quantities that no distinct crystal type could be identified. This was confirmed by the SwisensPoleno Jupiter classification, which also detected a large number of rimed particles. The Nakaya diagram, which was developed based on laboratory experiments, does not take riming conditions into account. Agreement is weaker for needles and columns. Ground observations of needle-shaped snowflakes are consistent, in terms of temperature range, with the Nakaya diagram, which predicts the formation of needles (a columnar shape) within a narrow temperature range around −5 °C. However, the observed humidity was slightly lower than the theoretical prediction. The classification, by contrast, predominantly identified columns, with a markedly lower proportion of needles. This discrepancy likely reflects the difficulty of the distinction itself rather than a genuine disagreement. Although the classification differentiates between needles and columns, the two belong to the same morphologically similar crystal family, with a gradual transition from columns to increasingly slender needles. This could lead to needles being classified as columns. Conversely, it is difficult to clearly distinguish between needles and columns by a simple visual observation, particularly when dealing with small crystals. The clearest deviation from observation to theory occurs in those time slots where the Nakaya diagram predicts columns but dendrites were observed instead. This mismatch suggests that

the visually observed crystals may not have formed in the immediate vicinity of the weather station but were transported from elsewhere. The crystal size of the observed dendrites (about 3 mm in diameter) supports this interpretation. Larger crystals imply a longer residence time in the cloud and, correspondingly, a greater transport distance, during which they would have been exposed to a range of different environmental conditions.

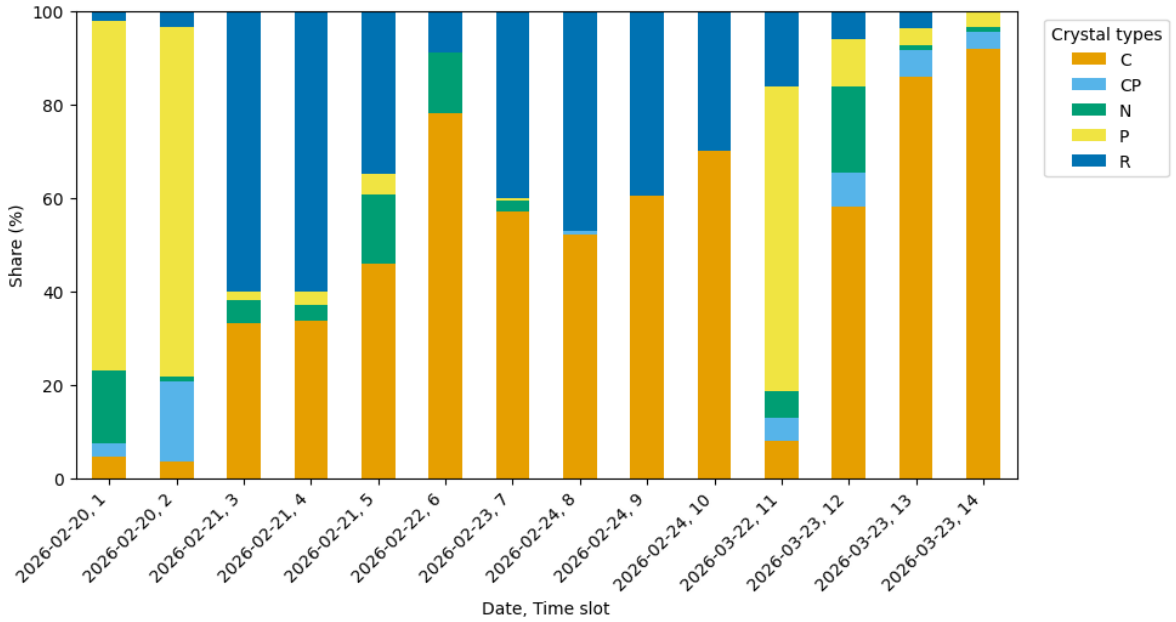


Figure 3: Distribution of the classified crystal types by time slot.

Table 2: Main crystal types SwisensPoleno Jupiter classification, observation and theory; T: temperature in 2 m, RH_w: relative humidity over water, P: plates, N: needles, R: rime, C: columns, D: dendrites, G: graupel.

No.	*Time slot [UTC]*	*Automatic weather station*		*SwisensPoleno Jupiter*		*Observation*		*Nakaya*
		T (°C)	*RH_w (%)*	*Main crystal types*	*Mean size Ø [µm]*	*Main crystal types*	*Size Ø [mm]*	*Crystal type*
1	2026-02-20 10:00-11:00	-14.2	87.8	P, N	50	P	1-2	P
2	2026-02-20 13:00-14:00	-13.3	87.6	P	50	P	1-2	P
3	2026-02-21 8:50-9:50	-9.5	89.0	R, C	-	D	3	C
4	2026-02-21 11:15-12:15	-9.8	86.5	R, C	-	D	3	C
5	2026-02-21 15:00-16:00	-9.9	90.0	C, R, N	35	D	3	C
6	2026-02-22 10:15-11:15	-4.7	94.5	C, N	43	N	2	C
7	2026-02-23 7:35-8:35	-7.5	90.2	C, R	32	G, D	1-2	C
8	2026-02-24 6:43-7:43	-6.6	92.0	C, R	39	R	1	C
9	2026-02-24 9:38-10:38	-6.3	92.2	C, R	38	D, N, R	1-2	C
10	2026-02-24 14:25-15:25	-6.6	92.2	C, R	37	N, D, R	1-2	C
11	2026-03-22 6:32-7:32	-11.6	88.0	P	62	D	3	P
12	2026-03-23 8:25-9:25	-11.3	87.8	C, N	36	D	3-4	P
13	2026-03-23 13:15-14:15	-9.0	88.1	C	33	D	2-3	C
14	2026-03-23 14:41-15:41	-9.2	88.8	C	31	D	4	C

Particularly noteworthy is the good agreement between the classification and the Nakaya diagram, with the notable exceptions of mainly rimed particles (time slot 3 and 4) and time slot 12, where columns instead of plates were predicted. To determine under which meteorological conditions the crystal forms

correspond, the data from the automatic weather station were averaged over the respective time period of each time slot and plotted on the Nakaya diagram (see Figure 4). Figure 4 shows that, for high relative humidity values over ice, the agreement is best.

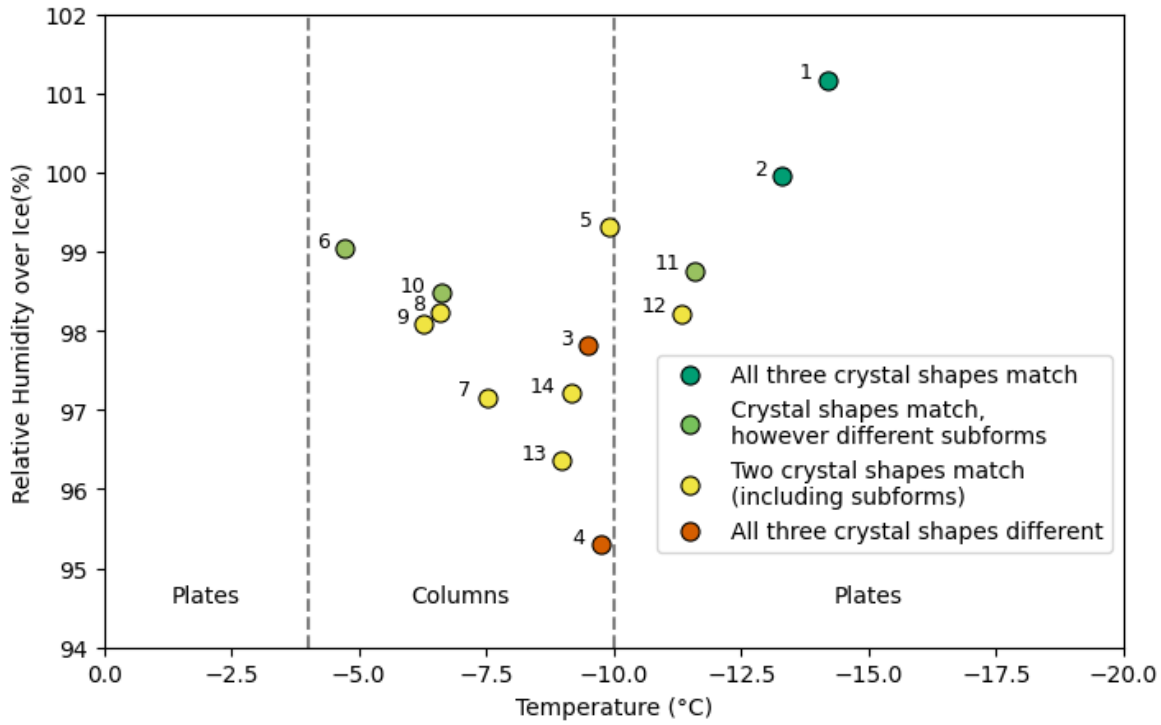


Figure 4: Consistency of the observed crystal forms during the observed time windows. Meteorological environmental conditions were averaged over the observation periods; transitions between plates and prisms are shown according to the Nakaya diagram (Nakaya, 1954).

4. DISCUSSION AND OUTLOOK

In conclusion, there are certain meteorological conditions under which the classification of the ice crystals, the visual observation of the snow flakes, and the Nakaya diagram align. In other cases, the observations differ significantly from the classification and the Nakaya diagram, primarily because the particles are transported within the cloud before they fall to the ground as snow. The observations then typically show dendrites, while the classification of the particles within the cloud and the Nakaya diagram indicate columnar crystals. However, classification and Nakaya diagram show an overall good agreement. This suggests that, based on the meteorological conditions, the shape of ice particles in the cloud can be predicted with a high degree of accuracy, whereas the shape of snow crystals falling to the ground can be predicted only when there is supersaturation over ice.

Crucial to the classification of ice crystals during numerous cloud events at SBO is the application of an automatic algorithm. This study provides a first approach towards achieving this. However, the classification results still need to be further verified. Although the method itself includes some quality checks, automatic classification processes always involve a certain degree of uncertainty. A next step to improve the results might be to use a larger training set. This might help especially to better distinguish between needles and columns, which remains a challenge due to their geometric similarity.

It would also be interesting to investigate other conditions characterized by ice supersaturation, under which crystal growth proceeds more rapidly and larger dendritic structures are favored. However, it remains an open question whether such larger dendrites can be reliably detected using the SwisensPoleno Jupiter device, as their size could exceed the range for which the device is designed.

ACKNOWLEDGEMENTS

We wish to express our sincere gratitude to the team at Sonnblick Observatory for their invaluable support in providing the photos of snowflakes and the associated data for this study. Their meticulous work and generous sharing of resources have greatly contributed to the depth and quality of our research.

Use of AI: AI-based tools were used to assist with language editing and the drafting of parts of the manuscript, as well as to support the development and debugging of code used in this work. All AI-generated content, including text and code, was independently reviewed, tested, and verified by the authors, who take full responsibility for the accuracy and integrity of the work.

REFERENCES

Bailey, M. and Hallett, J.: Growth Rates and Habits of Ice Crystals between −20° and −70°C, J. Atmospheric Sci., 61, 514–544, https://doi.org/10.1175/1520-0469(2004)061<0514:GRAHOI>2.0.CO;2, 2004.

Bailey, M. P. and Hallett, J.: A Comprehensive Habit Diagram for Atmospheric Ice Crystals: Confirmation from the Laboratory, AIRS II, and Other Field Studies, J. Atmospheric Sci., 66, 2888–2899, https://doi.org/10.1175/2009JAS2883.1, 2009.

Barrett, J. W., Garcke, H., and Nürnberg, R.: Numerical computations of faceted pattern formation in snow crystal growth, Phys. Rev. E, 86, 011604, https://doi.org/10.1103/PhysRevE.86.011604, 2012.

Demange, G., Zapolsky, H., Patte, R., and Brunel, M.: A phase field model for snow crystal growth in three dimensions, Npj Comput. Mater., 3, 15, https://doi.org/10.1038/s41524-017-0015-1, 2017.

Fuchs, C., Ramelli, F., Miller, A. J., Omanovic, N., Spirig, R., Zhang, H., Seifert, P., Ohneiser, K., Lohmann, U., and Henneberger, J.: Quantifying ice crystal growth rates in natural clouds from glaciogenic cloud seeding experiments, Atmospheric Chem. Phys., 25, 12177–12196, https://doi.org/10.5194/acp-25-12177-2025, 2025.

Furukawa, Y.: Snow and Ice Crystal Growth, in: Handbook of Crystal Growth, Elsevier, 1061–1112, https://doi.org/10.1016/B978-0-444-56369-9.00025-3, 2015.

Gravner, J. and Griffeath, D.: Modeling snow-crystal growth: A three-dimensional mesoscopic approach, Phys. Rev. E, 79, 011601, https://doi.org/10.1103/PhysRevE.79.011601, 2009.

Kobayashi, T.: The growth of snow crystals at low supersaturations, Philos. Mag., 6, 1363–1370, https://doi.org/10.1080/14786436108241231, 1961.

Krieger, V., Heuberger, A., Burkart, J., and Ludewig, E.: Relationship between ice fragments in clouds and precipitation particles during snow fall events in dependency of meteorological parameters – A case study at Sonnblick Observatory, Austria., in: Proceedings, International Snow Science Workshop, ISSW 2024, Tromsø, Norway, 2024.

Libbrecht, K. G.: Morphogenesis on Ice: The Physics of Snow Crystals, Eng. Sci., 64, 10–19, 2001.

Libbrecht, K. G.: The physics of snow crystals, Rep. Prog. Phys., 68, 855–895, https://doi.org/10.1088/0034-4885/68/4/R03, 2005.

Magono, C. and Lee, C. W.: Meteorological Classification of Natural Snow Crystals, J. Fac. Sci. Hokkaido Univ., 7, https://doi.org/10.14943/0016-7639.2.4.321., 1966.

Nakaya, U.: Snow Crystals: Natural and Artificial, Harvard University Press, https://doi.org/10.4159/harvard.9780674182769, 1954.

Pasquier, J. T., Henneberger, J., Korolev, A., Ramelli, F., Wieder, J., Lauber, A., Li, G., David, R. O., Carlsen, T., Gierens, R., Maturilli, M., and Lohmann, U.: Understanding the History of Two Complex Ice Crystal Habits Deduced From a Holographic Imager, Geophys. Res. Lett., 50, e2022GL100247, https://doi.org/10.1029/2022GL100247, 2023.

Reiter, C.: A local cellular model for snow crystal growth, Chaos Solitons Fractals, 23, 1111–1119, https://doi.org/10.1016/S0960-0779(04)00374-1, 2005.

Sauvageat, E., Zeder, Y., Auderset, K., Calpini, B., Clot, B., Crouzy, B., Konzelmann, T., Lieberherr, G., Tummon, F., and Vasilatou, K.: Real-time pollen monitoring using digital holography, Atmospheric Meas. Tech., 13, 1539–1550, https://doi.org/10.5194/amt-13-1539-2020, 2020.